Article



Organization and dynamics of cross-linked actin filaments in confined environments

Oghosa H. Akenuwa¹ and Steven M. Abel^{1,*}

¹Department of Chemical and Biomolecular Engineering, University of Tennessee, Knoxville, Tennessee

ABSTRACT The organization of the actin cytoskeleton is impacted by the interplay between physical confinement, features of cross-linking proteins, and deformations of semiflexible actin filaments. Some cross-linking proteins preferentially bind filaments in parallel, although others bind more indiscriminately. However, a quantitative understanding of how the mode of binding influences the assembly of actin networks in confined environments is lacking. Here we employ coarse-grained computer simulations to study the dynamics and organization of semiflexible actin filaments in confined regions upon the addition of crosslinkers. We characterize how the emergent behavior is influenced by the system shape, the number and type of cross-linking proteins, and the length of filaments. Structures include isolated clusters of filaments, highly connected filament bundles, and networks of interconnected bundles and loops. Elongation of one dimension of the system promotes the formation of long bundles that align with the elongated axis. Dynamics are governed by rapid cross-linking into aggregates, followed by a slower change in their shape and connectivity. Cross-linking decreases the average bending energy of short or sparsely connected filaments by suppressing shape fluctuations. However, it increases the average bending energy in highly connected networks because filament bundles become deformed, and small numbers of filaments exhibit long-lived, highly unfavorable configurations. Indiscriminate cross-linking promotes the formation of high-energy configurations due to the increased likelihood of unfavorable, difficult-to-relax configurations at early times. Taken together, this work demonstrates physical mechanisms by which cross-linker binding and physical confinement impact the emergent behavior of actin networks, which is relevant both in cells and in synthetic environments.

SIGNIFICANCE The actin cytoskeleton is vital for intracellular transport, yet it remains challenging to understand how its organization is impacted by the interplay between physical confinement and the cross-linking of semiflexible actin filaments. In this study, we explore how the mode of cross-linker binding and the aspect ratio of the confining region impact the assembly and organization of actin filaments. The dynamics are governed by rapid cross-linking of spatially proximal filaments into aggregates, followed by slower relaxation of their shape and connectivity. Indiscriminate cross-linking promotes more highly connected networks, greater curvature of long filament bundles, and a subset of filaments in highly unfavorable configurations. The results provide insight into mechanisms influencing the cytoskeleton in cells and in reconstituted systems.

INTRODUCTION

The actin cytoskeleton is a dynamic network of actin filaments that is essential for the function and growth of eukaryotic cells. In plant cells, it serves as scaffolding for active, myosin-driven transport with implications for biological processes such as the transport of mitochondria to areas of metabolic activity (1), the transport of Golgi stacks to growing pollen tubes and root hairs (2-4), and cytoplasmic

Submitted July 14, 2022, and accepted for publication November 28, 2022.

*Correspondence: abel@utk.edu Editor: Dimitrios Vavylonis.

https://doi.org/10.1016/j.bpj.2022.11.2944

© 2022 Biophysical Society.

streaming (5). Despite the importance of actin networks in many cellular processes, it remains challenging to understand how their organization and dynamics are regulated by both biochemical and physical factors.

Actin filaments are often physically restricted within confined regions. For example, in plant cells, the cell wall provides rigid external confinement, and the large vacuole can occupy up to 90% of the cytoplasm, leading to quasi-2D environments between the vacuole and plasma membrane. The shape of cells varies based on type, leading to different confining shapes. Some cells, like root hairs and pollen tubes, are highly extended in one dimension and have large aspect ratios. Additionally, actin cross-linking



proteins (ACPs) physically cross-link actin filaments in a reversible manner. Both reconstituted in vitro experiments and computer simulations have provided insight into the dynamics and organization of actin networks. However, much remains unknown about how they are impacted by physical confinement and properties of ACPs. In this work, we investigate confined regions of different aspect ratios and the mode of binding of the cross-linker (whether restricted to cross-linking locally aligned filaments or indiscriminate in binding). Given the wide variety of cross-linking proteins and cellular shapes, this has the potential to inform understanding of actin networks in both cellular and reconstituted

In cells, ACPs help to organize actin networks, contributing to the formation of functional structures such as lamellar networks, filopodial cables, asters, and contractile bundles (5-7). How ACPs bind to actin filaments influences the structure and properties of the actin network (8–11). Some ACPs, such as fascin and plant villin, cross-link actin filaments that are aligned in the same direction. Other ACPs, such as α -actinin and filamin, are promiscuous cross-linkers that cross-link filaments regardless of their relative orientation (5,12). ACPs that cross-link filaments in parallel promote the formation of bundles containing filaments parallel to one another (5,13,14). Bundles of filaments can further influence the structure of the network because they have a larger bending stiffness than single filaments (13). Promiscuous cross-linkers promote the formation of meshwork networks comprised of both bundles and individual filaments (9,15). However, most experimental work studying the effects of cross-linking proteins on actin networks has examined reconstituted bulk systems in which confinement does not play a role.

Computational studies have provided additional insight into the effect of ACPs on the organization of actin filaments. Most have used coarse-grained approaches where cross-linkers were modeled either as an implicit attractive force between filaments (16–19) or as a spring with explicit cross-linker-actin binding interactions (20-25). Recent approaches include MEDYAN (mechanochemical dynamics of active networks), a coarse-grained stochastic reactiondiffusion scheme (26), and AFINES (active filament network simulation), a hybrid kinetic Monte Carlo and Brownian dynamics method (20,27–29). Both methods have been used to simulate cytoskeletal networks with cross-linking proteins and molecular motors. Two recent studies (28,29) used AFINES to study actin networks cross-linked with both fascin (restricted) and α -actinin (unrestricted). These studies focused on sorting of cross-linkers into domains on actin bundles and within the network. Cyron et al. (22) also considered preferred binding angles of cross-linked filaments, but their focus was constructing an equilibrium phase diagram when cross-linkers were limited to binding filaments at specific angles.

Both experimental and computational efforts have shown that confinement can modulate the organization of actin filaments even in the absence of cross-linking proteins. Experimental studies in vitro have examined the organization of actin filaments in confined regions such as microfabricated shallow chambers (30–32) and vesicles (9,33–36). Theoretical studies have shown the formation of coils and loops by long semiflexible filaments in spherical cavities (37,38). Relatively few studies have examined the effect of both confinement and cross-linking on actin networks. Combining actin with fascin in micropatterned, quasi-2D chambers produces bundles that tend to align with the longest axis of the confinement (32). Deshpande and Pfohl studied reconstituted actin networks in quasi-2D chambers (39), showing that the bundling agent and filament length strongly influence the organization of actin filaments. Short filaments form compact, isolated bundles, whereas long filaments form a network of highly deformed, interconnected bundles. Koudehi et al. simulated actin networks with implicit attraction between polymers in spherical confinement (40). Their results showed the formation of loops, rings, and bundle structures depending on the average filament length and the strength and range of the implicit attraction.

This paper investigates the combined effects of crosslinking and confinement on actin networks. We focus on two physical features that, to our knowledge, have not been studied together using computational methods: the shape of the region confining the actin filaments and whether cross-linkers bind in a restricted or indiscriminate manner. We extended the AFINES model originally developed by Freedman et al. (20) to account for different types of cross-linker binding. In the paper, we first give a brief overview of the computational methods and then explore the impact of system shape (square versus rectangular domains), mode of cross-linker binding, number of crosslinkers, and filament length. We show the impact on network organization and analyze the connectivity of the networks using graph-theoretic tools. We then characterize various measures of the dynamics and analyze the bending energy of filaments to gain insight into deformations of filaments. We discuss the results in the context of how system shape and the mode of cross-linker binding impact the dynamics and organization of actin networks.

METHODS

Computational framework

We used the AFINES model, developed by Freedman et al. (20,27,28), which is a coarse-grained model that uses kinetic Monte Carlo and Brownian dynamics to simulate actin filaments and cross-linkers. For this work, we utilized the model to study cross-linkers with different binding properties, which we imposed as a potential energy term associated with the relative local orientation of cross-linked filaments. We provide a brief overview of the method, details of which can be found in Freedman

In the AFINES model, actin filaments are modeled as semiflexible, beadspring polymers in two dimensions. One end of the filament represents the barbed (plus) end, and the other represents the pointed (minus) end. For a filament with N beads and N-1 links, the potential energy is given by $U_{\rm f} = U_{\rm f}^{\it stretch} + U_{\rm f}^{\it bend}$, where

$$U_{\rm f}^{\rm stretch} = \frac{k_f}{2} \sum_{i=1}^{N-1} \left(\left| \vec{r}_{i+1} - \vec{r}_i \right| - l_a \right)^2$$

$$U_{\rm f}^{\rm bend} = \frac{\kappa_B}{2l_a} \sum_{j=1}^{N-2} \theta_j^2 \tag{1}$$

Here, \vec{r}_i is the position of the i^{th} bead on the filament, l_a is the equilibrium spring length, k_f is the spring constant for stretching, κ_B is the bending modulus, and θ_j is the angle between the j^{th} and $(j+1)^{th}$ link. Excluded volume interactions are neglected. The bending modulus is chosen so that the persistence length of an isolated actin filament is 17 μ m.

Cross-linkers are treated as Hookean springs with two ends (heads) that can stochastically bind and unbind from filaments. The energy of a crosslinker is given by $U_{xl} = U_{xl}^{stretch} + U_{xl}^{bind}(I_1 + I_2) + U_{xl}^{align}$, where

$$U_{xl}^{stretch} = \frac{k_{xl}}{2} \left(\left| \vec{r}_1 - \vec{r}_2 \right| - l_{xl} \right)^2$$

$$U_{xl}^{bind} = -k_B T \ln \left(k_{xl}^{on} / k_{xl}^{off} \right)$$

$$U_{xl}^{align} = \frac{1}{2} k_{align} (\theta - \theta_0)^2$$
(2)

are contributions from stretching, binding to filaments, and misalignment of cross-linked filament links. Here, l_{xl} is the equilibrium length of the crosslinker, $k_{\rm xl}$ is its stretching stiffness, and $I_{\rm m}$ is 1 if head m is bound and 0 otherwise. k_{xl}^{on} and k_{xl}^{off} are the binding and unbinding rates respectively. For values of the parameters, we refer the reader to Freedman et al. (27).

In this work, we incorporate an angular harmonic potential, U_{x1}^{align} , to penalize cross-linked filaments that are not locally aligned. Here, θ is the angle between cross-linked filament links (Fig. 1) and $\theta_0 = 0$. For restricted cross-linkers, which preferentially bind locally-aligned filaments, $k_{align} = 0.011$ pN μ m. For unrestricted cross-linkers, which bind indiscriminately with respect to filament orientation, $k_{align} = 0$. This approach is conceptually similar to that used in Freedman et al. (28) and Bashirzadeh et al. (29), where there is a potential that promotes cross-linkers being perpendicular to the filament link associated with each head. Cross-linkers impose forces on filaments when they are concurrently bound to two filaments. This force acts on the actin beads of the filament links and is calculated in accordance with standard methods (41). When filament links i and jare cross-linked, the force due to the alignment potential acts on each of the actin beads (a) associated with their endpoints and is given by

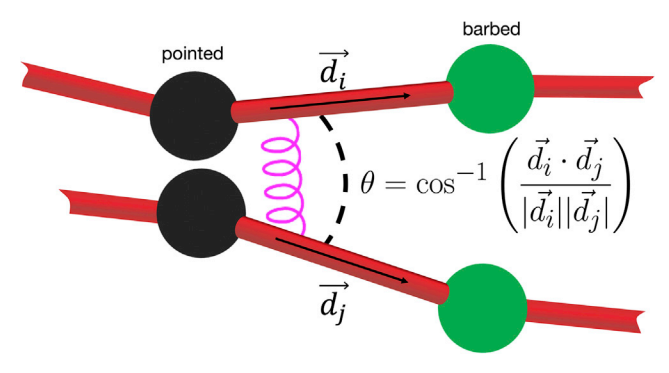


FIGURE 1 Schematic showing the definition of θ , the angle between two cross-linked filament links, used in U_{x1}^{align} . To see this figure in color, go online.

$$F_a = -\nabla_{r_a} U_{xl}^{align} = -\left(\frac{\mathrm{d}U_{xl}^{align}}{\mathrm{d}\cos\theta}\right) \nabla_{r_a}\cos\theta, \quad (3)$$

where r_a denotes the position of the actin bead, $\cos \theta = \vec{d}_i \cdot \vec{d}_i / |\vec{d}_i| |\vec{d}_i|$, and \vec{d}_k is the displacement vector of filament link k. Additionally, when both cross-linker heads are bound to filaments, tensile forces due to compression or stretching of the cross-linkers are propagated to the filament beads using a lever rule (24).

Dynamics are governed by a kinetic Monte Carlo arm to update the binding and unbinding of cross-linkers and a Brownian dynamics arm to update the positions of particles in the system. The simulations satisfy the detailed balance condition, as discussed in Freedman et al. (20). The system is updated at discrete times with the interval $\Delta t = 10^{-4}$ s. Given a state of the system, each unbound cross-linker head binds to accessible filament links with probability $k_{on}\Delta t \min[1, \exp(-(\Delta U_{\text{H} \to \text{b}})/k_{\text{B}}T)]$. Each bound head unbinds with probability $k_{off}\Delta t \min[1, \exp(-(\Delta U_{b\to u})/k_BT)]$. Here, $\Delta U_{\rm u} \rightarrow {}_{\rm b}$ denotes the difference in stretching and alignment energy between the bound (new) and unbound (original) state, $\Delta U_{\rm u \rightarrow b} = \Delta U_{\rm xl,u \rightarrow b}^{stretch} +$ $\Delta U_{\rm xl,u \to b}^{align}$. Similarly, $\Delta U_{\rm b \to u}$ denotes the difference between the unbound and bound state. Then, given the updated state of the system, positions of the filament beads and the cross-linker heads are updated using overdamped Langevin dynamics, propagating the time forward by Δt . The process is then repeated.

Parameters studied

We considered filament lengths of L = 10, 5, and $2 \mu m$. The number of filaments (N_f) was varied to keep the total filament length constant across all simulations ($N_f L = 1000 \, \mu \text{m}$). The number of cross-linkers was varied, with $N_c = 206, 412, 825, 1650$, and 3300. Two confinement shapes were examined: a square box of size 20 μ m \times 20 μ m and a rectangular box of size 40 μ m \times 10 μ m. These dimensions are typical of quasi-2D environments found in plant cells. For comparison, we considered additional system sizes, aspect ratios, and shapes, as specified in the text.

All simulations were initialized by randomly distributing filaments in the system and allowing them to equilibrate without cross-linkers for 400 s. Unbound cross-linkers were then added uniformly at random, and the simulations were continued for an additional 400 s. Reflective wall boundary conditions were imposed to simulate confinement of the actin network. For each simulation condition, three independent simulation trajectories were generated and analyzed.

RESULTS AND DISCUSSION

In our simulations, we systematically varied the length of actin filaments, the number and type of cross-linkers, and the shape of confinement (square versus rectangular). To illustrate typical behavior, Fig. 2 shows snapshots taken from a trajectory with 100 filaments ($L = 10 \,\mu\text{m}$) and 1650 cross-linkers (unrestricted binding, $k_{align} = 0$). A corresponding video is available (Video S1). The trajectory exhibits an initial regime in which cross-linkers rapidly bind to filaments, cross-linking those initially in close proximity (compare t = 0 and 10 s). This is followed by a regime of slower relaxation in which individual filaments and bundles of filaments rearrange and coalesce, forming larger, well-defined bundles of filaments. After 400 s, the network is characterized by highly connected filaments that form several large bundles, which are curved and form loops in

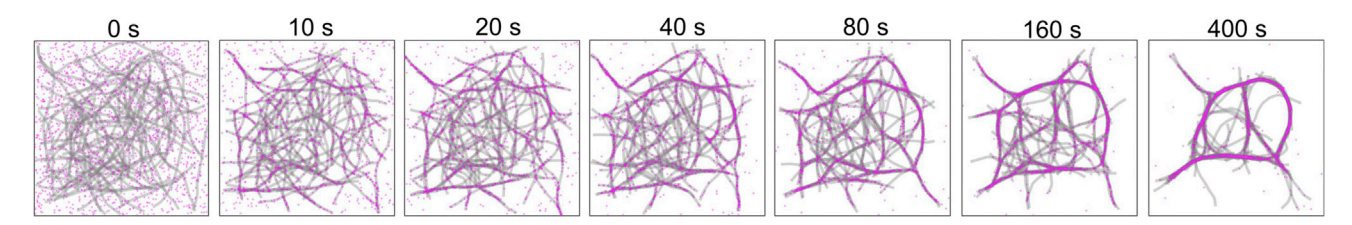


FIGURE 2 Snapshots showing the time evolution of a network with 10-μm filaments and 1650 unrestricted cross-linkers in a 20 μm × 20 μm domain. Filaments are shown in gray and cross-linkers in fuchsia. A corresponding video is available (Video S1). To see this figure in color, go online.

the network structure. A relatively small number of filaments are only partially cross-linked to the large bundles.

Network organization and filament bundling

Square confinement

Fig. 3 shows snapshots taken from simulation trajectories in square confinement 400 s after introducing cross-linkers. The snapshots illustrate filament configurations obtained by varying filament length, the number of cross-linkers, and the alignment potential. Bundles consisting of many filaments are highlighted by the large number of cross-linkers associated with them. Fig. S1 shows an alternative depiction of filaments that is analogous to an imaging experiment in which fluorophores are uniformly distributed along filaments. This highlights the local density of filaments.

Generally, as the number of cross-linkers increases, there is more pronounced aggregation of filaments into welldefined bundles of filaments. For small numbers of crosslinkers (206 and 412), there are localized aggregates of filaments that form bundle-like structures with longer filaments. For intermediate numbers of cross-linkers (825), most filaments are cross-linked into a small number of bundles. For larger numbers of cross-linkers, the bundles become better defined, with fewer filaments only partially connected to the bundles.

The shortest filaments (2 µm) form short, isolated aggregates at intermediate and large numbers of cross-linkers. The filaments and aggregates are short compared with the confining dimensions, so the walls have little impact on their shape or their orientation. The number of distinct aggregates is larger with restricted cross-linker binding (Fig. 3 A) than with unrestricted binding (Fig. 3 B). This is because restricted binding prevents nearby aggregates with different orientations from easily cross-linking; it also decreases the likelihood for "spanning" filaments to connect nearby aggregates at shorter times. Further aggregation is dependent on fluctuations that change the position and orientation of aggregates, which is a relatively slow process.

Longer filaments (5 and 10 μ m) are more significantly impacted by confinement because they form bundled structures with lengths that exceed those of individual filaments. In these cases, the presence of confining surfaces influences the organization of the filament assemblies and leads to curvature of individual filaments and bundles. With large numbers of cross-linkers, there is an increase in the curvature of the bundles and the emergence of loops in the network structure. These features are more pronounced with unrestricted cross-linking and emerge at a smaller number of cross-linkers for 10-µm filaments compared with $5-\mu m$ filaments.

Rectangular confinement

Fig. 4 shows snapshots from simulation trajectories in rectangular confinement. The cases are directly comparable to those in Fig. 3 and demonstrate the impact of the system

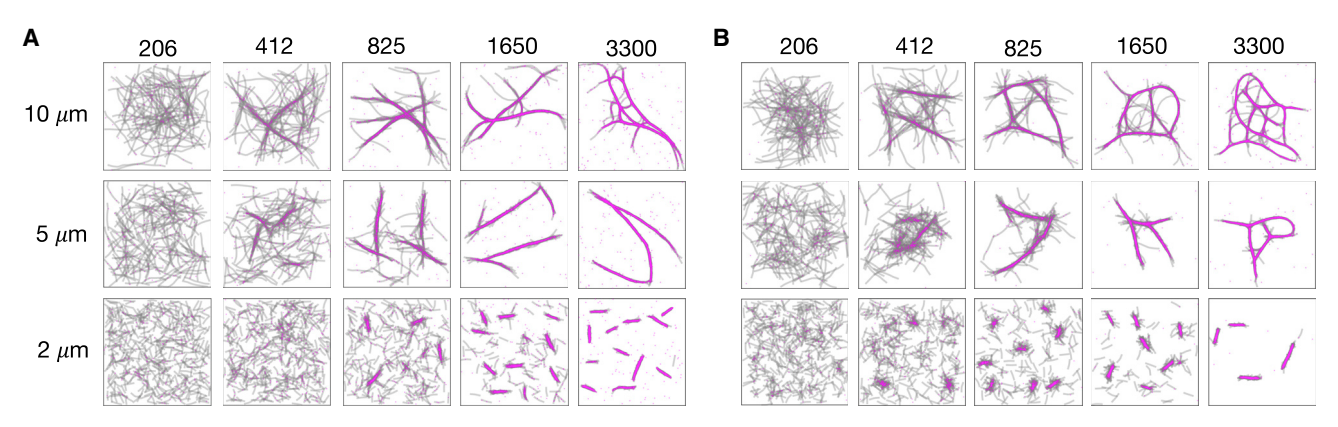


FIGURE 3 Snapshots of networks at 400 s in square confinement (20 μ m \times 20 μ m) with restricted cross-linkers (A) and unrestricted cross-linkers (B). Results are shown for different filament lengths and numbers of cross-linkers. Filaments are shown in gray and cross-linkers in fuchsia. An alternative depiction showing only the filaments can be found in Fig. S1. To see this figure in color, go online.

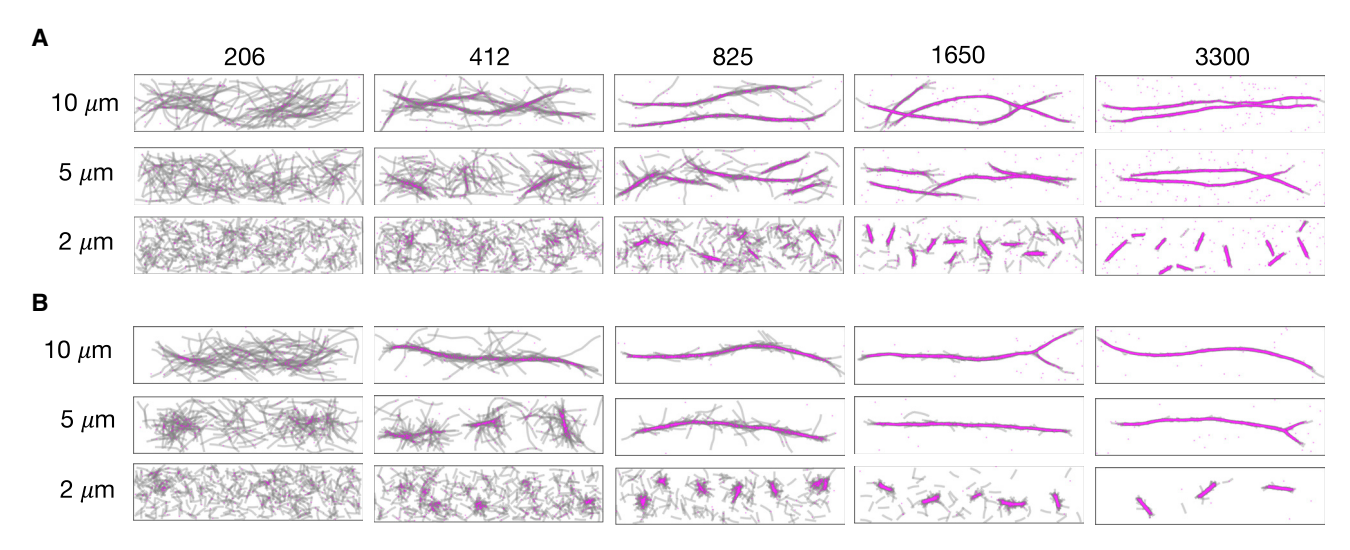


FIGURE 4 Snapshots of networks at 400 s in rectangular confinement (40 μ m \times 10 μ m) with restricted cross-linkers (A) and unrestricted cross-linkers (B). Results are shown for different filament lengths and numbers of cross-linkers. Filaments are shown in gray and cross-linkers in fuchsia. An alternative depiction showing only the filaments can be found in Fig. S1. To see this figure in color, go online.

shape. With 5- and 10- μ m filaments, the rectangular domain induces strong alignment of the filaments with its long dimension when the filaments are cross-linked into bundles. The alignment is quantified in Fig. S2, which shows the distribution of angles of filament links relative to the long axis of the system.

With restricted cross-linking (Fig. 4 A), the filaments coalesce into two main bundles with filaments that are oriented in opposite directions. The restricted binding prevents the bundles from coalescing. The 5 μ m filaments require more cross-linkers to induce elongated bundles and strong orientational ordering of the filaments. With unrestricted cross-linking (Fig. 4 B), small numbers of cross-linkers result in larger aggregates. Larger numbers of cross-linkers result in a single aligned bundle with a length comparable to the long dimension of the simulation box.

We characterized the impact of the aspect ratio of the confining region by varying the aspect ratio of the rectangular domain while keeping the area constant (Fig. S3). For 5- and 10- μ m filaments, as the aspect ratio increases, the filaments gradually become more aligned with the long axis.

Analysis of network connectivity

To characterize connectivity of the actin networks, we represented each network as a graph in which filaments were represented as nodes. Two nodes were connected by an edge if the two corresponding filaments were cross-linked. From each graph, we parsed filaments into communities based on connectivity of the graph using the fast Newman greedy algorithm (42). The basis for the algorithm is that filaments have more connections with other filaments within their community than with filaments outside their community.

Fig. 5 shows graphs depicting the connectivity of the filament networks with $10-\mu m$ filaments. The nodes are colored according to their community, and corresponding snapshots are shown with the filaments colored by community. This illustrates that communities are typically associated with aggregates or bundles of filaments. Figs. S4 and S5 show the graphs associated with all varied parameters (L, N_c) and type of cross-linker).

With restricted cross-linkers, increasing the number of cross-linkers first leads to isolated aggregates, followed by larger bundles of filaments. With the 10 μ m filaments shown, large numbers of cross-linkers result in a fully connected graph, indicating that the bundles identified by community analysis are connected by filaments spanning between them. With unrestricted cross-linkers, small numbers of cross-linkers lead to more filaments being linked, and fully connected networks emerge with smaller numbers of crosslinkers. This is because the relative orientation of filaments does not impact binding, facilitating connections.

Variation of the simulation domain

Our simulations were conducted with a fixed area $(400 \, \mu \text{m}^2)$. To characterize the impact of system size, we varied the size of the square domain with fixed concentrations of filaments and cross-linkers. We examined side lengths of 10, 20, 30, and 50 μ m. For the largest system, we used periodic boundary conditions. Snapshots of resulting networks after 400 s are shown in Figs. S6 and S7. For the smaller systems, bundles tend to align along the diagonal of the system, and network structures containing large deformations and loops are rarely observed. In contrast, for the larger systems, large connected structures consisting of cross-linked bundles emerge with no apparent preferred orientation. These observations are

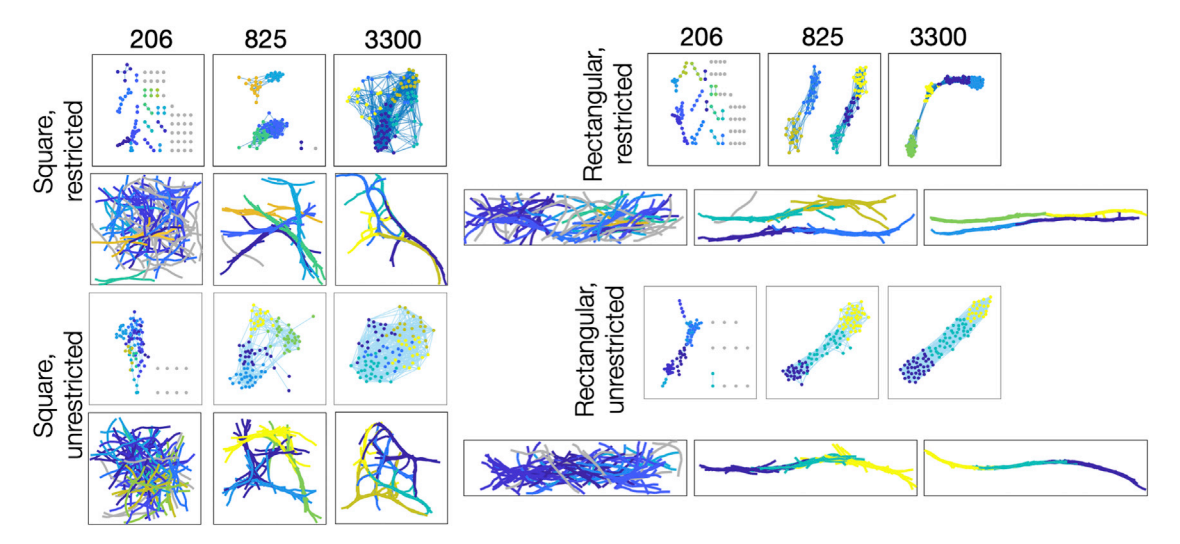


FIGURE 5 Graphs and corresponding snapshots depicting the connectivity of networks with 10-μm filaments for different domain shapes and types of cross-linkers. Cases are shown with 206, 825, and 3300 cross-linkers. Each node represents a filament, and each link represents cross-linking between two filaments. Nodes and corresponding filaments are colored according to the community determined based on the connectivity. Nodes and filaments that are not cross-linked are shown in gray. To see this figure in color, go online.

quantified by the distributions of angles between filament links and the horizontal axis (Fig. S8).

We also considered confinement within a circular domain with an area 400 μ m². A confining potential of the same form as Bashirzadeh et al. (29) was used to confine the network (see supporting material for details). Snapshots of resulting networks are shown in Fig. S9 A and B, and they are qualitatively similar to square confinement at equivalent conditions. However, there is no preferred orientation of isolated bundles as is observed along the diagonal of square domains. Additionally, with large numbers of cross-linkers, circular confinement leads to a more compact network with 5- and 2- μ m filaments (Fig. S9 C). This is likely due to differences in the distribution of distances between filaments in square and circular confinement.

Dynamics of aggregation and network relaxation

Area fraction occupied by filaments

The trajectory shown in Fig. 2 (Video S1) illustrates that the cross-linking of filaments at short times impacts the subsequent relaxation and coarsening. Videos S2, S3, and S4 show additional cases with the same numbers of filaments (100) and cross-linkers (1650) but that vary in cross-linker type and confinement shape. In all cases, cross-linkers lead to aggregation and bundling of filaments, but the dynamics are impacted by the type of cross-linker and the shape of confinement.

Aggregation of filaments leads to larger expanses of space without filaments. To quantify this, we computed the area fraction occupied by filaments as a function of time. The area fraction was determined by dividing the simulation box into square voxels with a side length of 0.1 μ m and determining the fraction of voxels containing a filament. The area fraction reported for each case is averaged over three simulation trajectories (Fig. 6). Increasing the number of cross-linkers leads to a larger decrease in the area fraction occupied by filaments over time. This is consistent with Figs. 3 and 4, with more cross-linkers promoting a higher degree of bundling. When sufficiently large numbers of cross-linkers are present, the general response is characterized by fast initial decay followed by slower decay at longer times. It is clear that many of the systems are not equilibrated after 400 s and that the area fraction would continue to decrease at longer times.

Fig. 6 also quantifies the impact of the type of cross-linker on the dynamics. With 206 cross-linkers (not shown), there is little change in the filament area fraction over time. With larger numbers of cross-linkers and 2-µm filaments, unrestricted cross-linking leads to a faster and more pronounced decrease in the filament area fraction compared with restricted cross-linking. For longer filaments, restricted cross-linkers lead to more pronounced decay of the filament area fraction at early times. However, there is a crossover point after which unrestricted cross-linkers lead to a lower filament area fraction (except for 10-\mu m filaments in square confinement, where this would presumably occur at later times). This suggests that unrestricted cross-linking leads to frustration at early times due to the promiscuous crosslinking of filaments that is then slow to relax.

Connectivity of filaments

The area fraction occupied by filaments characterizes the spatial distribution of filaments, but it does not directly measure their connectivity. We therefore used the community analysis discussed above to characterize the evolving connectivity of the filaments. Fig. 7 shows the number of

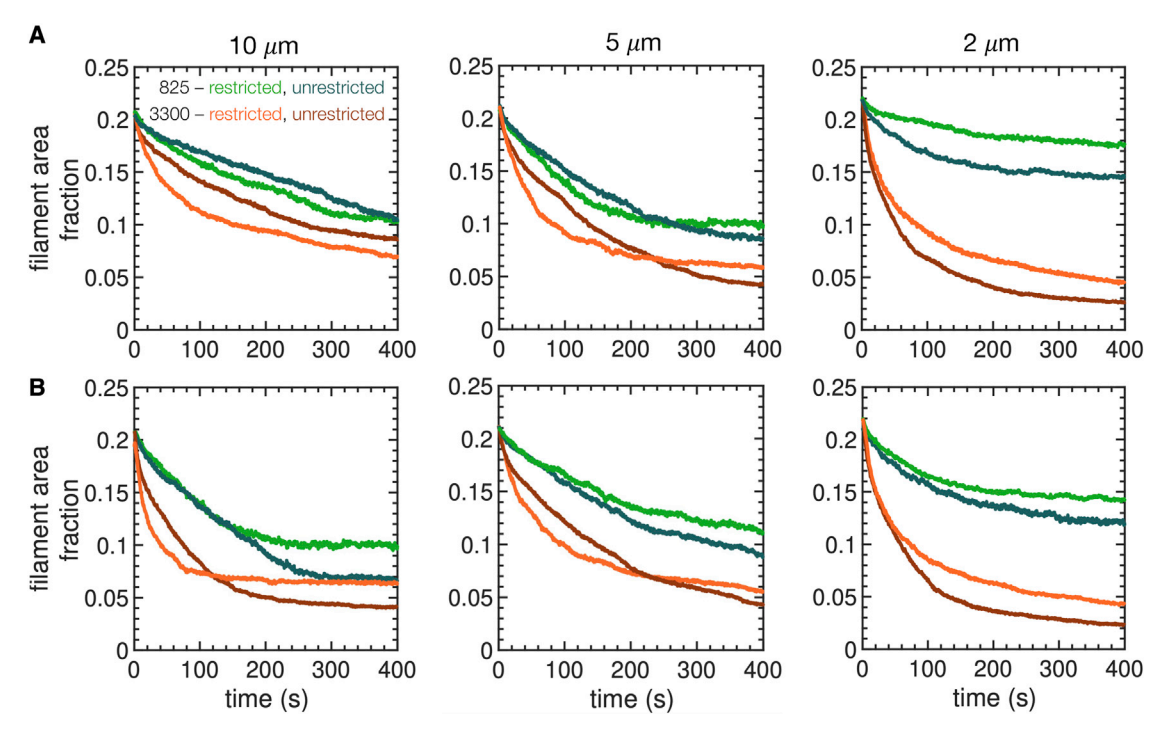


FIGURE 6 Area fraction occupied by filaments over time in square (A) and rectangular (B) domains. Curves are shown for both restricted and unrestricted cross-linkers with $N_c = 825$ and 3300. Each curve is averaged over three simulation trajectories. To see this figure in color, go online.

communities as a function of time for the case with 3300 cross-linkers. After a rapid increase, the number of communities decreases over time. This corresponds to the rapid initial cross-linking of nearby filaments followed by their longer-term aggregation and rearrangement.

Unrestricted cross-linkers cause a rapid "overshoot" in the number of communities at short times, followed by a rapid decrease in the number of communities. In contrast, restricted cross-linkers give rise to a maximum value at a slightly later time and remain plateaued around that value for a longer time. Additionally, the maximum value is larger for restricted cross-linkers. These features are consistent with the relative ease by which unrestricted cross-linkers can bind: more filaments are directly connected at short times, leading to fewer communities. Additionally, the number of communities decays rapidly because filaments can be cross-linked and bundled regardless of orientation. In contrast, with restricted cross-linking, the initial connectivity gets "locked in" because nearby filaments oriented in different directions have to reorient before being crosslinked.

We further characterized the connectivity within communities (Fig. S10). The average number of cross-linkers between any two filaments in a community increases to a maximum at early times, and then it decreases. Further, the average fraction of filaments in a community to which one filament is connected increases at early times, indicating a dynamic change in the connectivity of networks. Short filaments and rectangular confinement promote the decrease of this value at later times, likely indicating the coalescence of initially separated bundles that are then connected in a relatively sparse manner.

Physical interpretation

Differences in dynamical signatures are rooted in the interplay between cross-linker binding, filament length, and subsequent relaxation dynamics. Physically, the promiscuous binding of unrestricted cross-linkers makes it easier for nearby filaments to be cross-linked because rearrangement is not required when the filaments are not aligned. This leads to fast dynamics for short filaments because they quickly form short, bundled aggregates of nearby filaments. However, unrestricted binding can cross-link long filaments into unfavorable or hard-to-relax configurations at short times. This slows the dynamics because further relaxation relies on collective effects such as the unbinding of multiple cross-linkers or large-scale rearrangements of filaments and bundles.

Bending energy of cross-linked filament networks

Average bending energy of filaments

The previous results show restricted and unrestricted crosslinkers lead to differences in the curvature of bundles (Figs. 3 and 4) and in the dynamics of aggregation (Fig. 6). These results suggest that filaments can be cross-linked in unfavorable configurations, which slows the relaxation of the

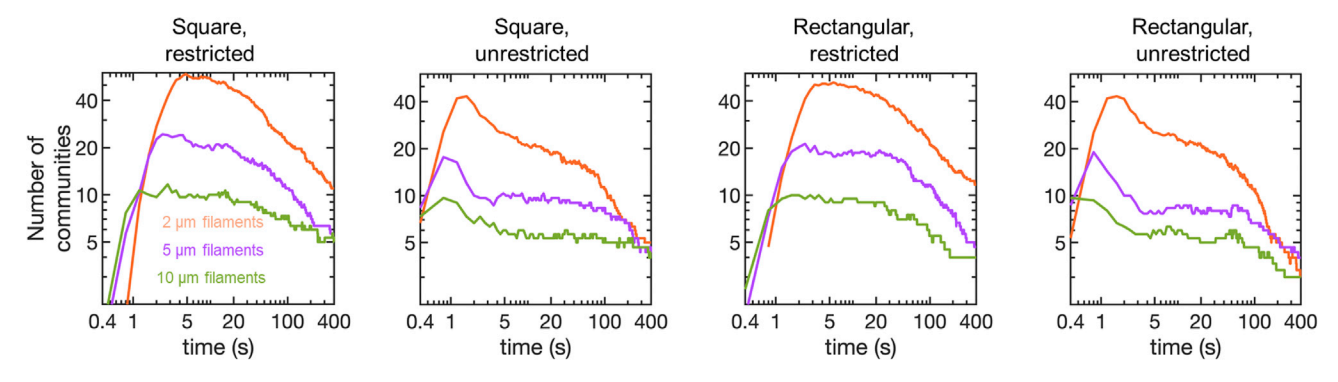


FIGURE 7 Number of communities over time. Results are shown for different filament lengths, domain shapes, and types of cross-linker. All cases have 3300 cross-linkers. Each curve is averaged over three simulation trajectories. To see this figure in color, go online.

network. To gain more insight into the configurations induced by cross-linking, we measured the bending energy of filaments over time as a measure of their deformations. Fig. 8 shows the average bending energy per filament over time for various conditions. The cases with 206 and 412 cross-linkers produced similar results, so we omitted the case with 206 cross-linkers for clarity. The average bending energy per filament in the absence of cross-linkers is given by the value at t = 0 s.

We begin by discussing 2- μ m filaments because they illustrate the influence of cross-linkers without complications introduced by strong coupling between bundles or by confinement effects. For this case (Fig. 8), the mean energy decreases with increasing number of cross-linkers. This is because the filaments form short, straight bundles. Crosslinking suppresses fluctuations in the shapes of individual filaments, thus decreasing the average bending energy. The average bending energy with restricted binding is lower than with unrestricted binding because the alignment potential promotes alignment and further suppresses shape fluctuations. The difference between square and rectangular confinement is negligible because of the short length of the aggregates.

For longer filaments, Fig. 8 reveals two key takeaways: 1) bending energies are typically higher with unrestricted cross-linkers than with restricted, and 2) square confinement results in higher bending energies than rectangular confinement. Small numbers of cross-linkers lead to a modest, monotonic decrease in the average bending energy. This is driven by suppressed fluctuations of cross-linked filaments. With larger numbers of cross-linkers, there is more pronounced cross-linking between different bundles, which are also long enough to be impacted by confinement. Here the behavior of the average bending energy is more complex, with increasing numbers of cross-linkers leading to less pronounced decay or even increasing energy over time (leading to nonmonotonic behavior in some cases). This behavior is more pronounced for unrestricted crosslinking and square confinement. Both of these cases promote cross-linking between different bundles of filaments and unfavorable filament configurations. Networks confined in circular domains exhibit average filament energies similar to the square domains (Fig. S9 D and E).

It was surprising to observe long-lived elevated bending energies in the rectangular domain (Fig. 8) because the filaments appear to form well-organized and straight bundles (Fig. 4 A and B). This suggests that even though the network forms relatively straight bundles, some filaments are in highly unfavorable configurations.

Bending energy of individual filaments

To further explore the behavior of individual filaments, we show the bending energy of each filament over the course of a single trajectory in Fig. 9 A. We focus on $10-\mu m$ filaments with 3300 cross-linkers to illustrate the underlying physics. By inspection, a relatively small proportion of the filaments have markedly larger bending energies than the other filaments. To quantify this, at each timepoint we characterized "outlier filaments" as having bending energies above the upper fence of the overall distribution of bending energies (= Q3 + 1.5(Q3 - Q1), where Q3 and Q1denote the upper and lower quartile of the distribution, respectively). The energies of filaments characterized as outliers at 200 s are shown in non-gray colors.

In square confinement with restricted cross-linking (Fig. 9 A), the energies of outlier filaments gradually increase over time, suggesting a slow change in the configuration of the overall network. In contrast, outliers in the other cases commonly reach sustained plateau values, suggesting long-lived, unfavorable configurations of individual filaments. Many of these rapidly switch from their high-energy state to a lower, "typical" bending energy. This indicates rapid relaxation of an individual filament from an unfavorable to a favorable configuration, which is mediated by the unbinding of cross-linkers. These observations are consistent with the average bending energy of filaments with and without the outlier filaments included (Fig. S11). With restricted cross-linkers, the typical filaments plateau at a smaller average bending energy than unrestricted cross-linkers. The outlier filaments continue to increase in

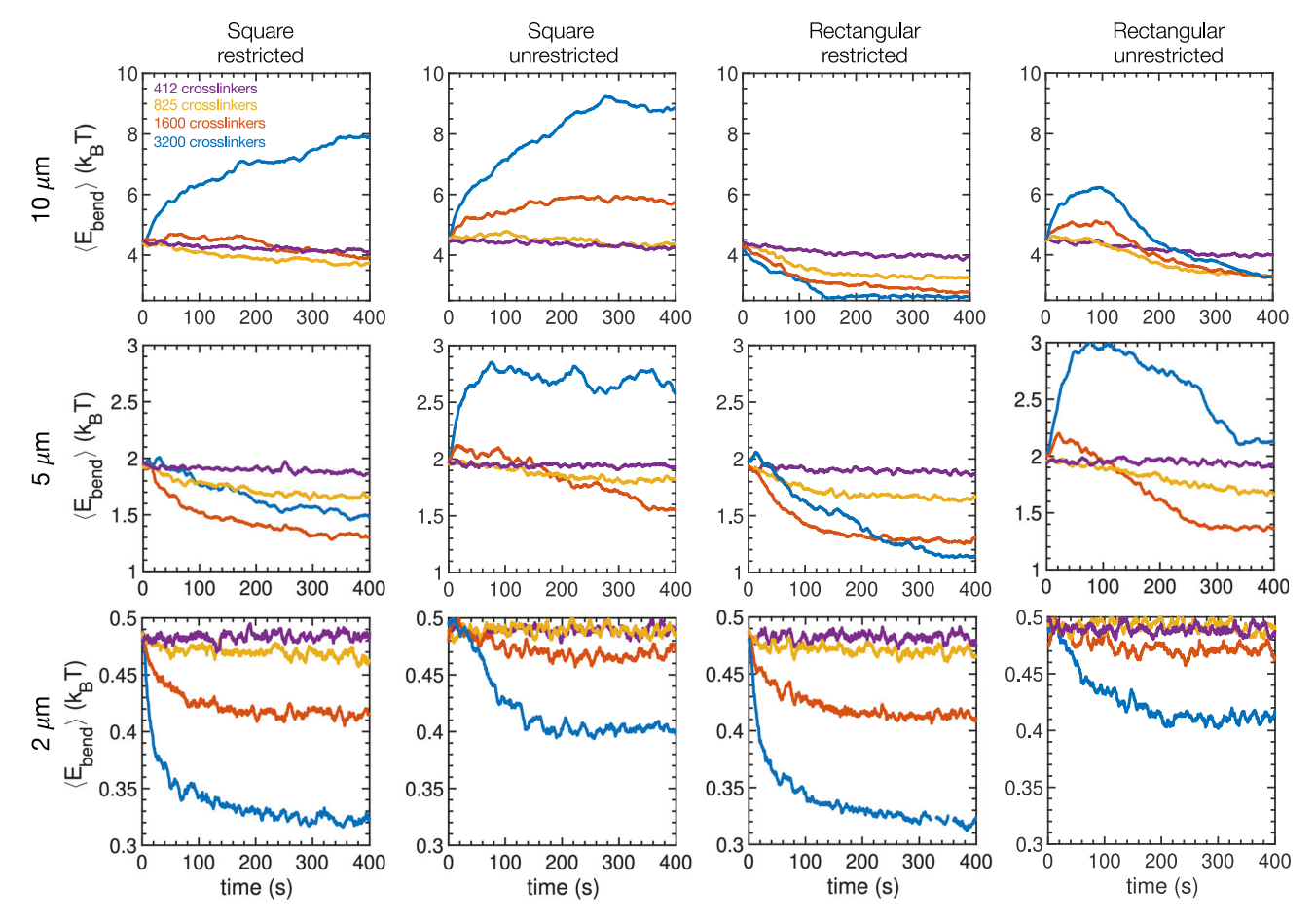


FIGURE 8 Mean filament bending energy over time. Results are shown for different filament lengths, confinement shapes, and types of cross-linker. Each curve is averaged over three simulation trajectories and, for clarity, is presented as a moving average with a time window of 8 s. To see this figure in color, go

average bending energy, which is consistent with bundles forming early, followed by their long-time relaxation leading to an increase in energy of filaments spanning the bundles.

Fig. 9 B shows snapshots taken from the trajectories in Fig. 9 A. Each snapshot depicts the filament configuration at 200 s, with the outliers shown in the same color as in Fig. 9 A. For the square domain with restricted cross-linking, the filaments with highest bending energy each span at least two distinct bundles and adopt a horseshoe-like shape. With unrestricted cross-linking, the outliers fall into two groups: a high-energy group with $E_{bend} \approx 60 k_B T$ and a lower-energy group. The highest-energy filaments are distinguished by sharp, hairpin-like turns, whereas the lower-energy group are characterized by less severe deformations.

In rectangular confinement, restricted cross-linking leads to a small number of horseshoe-like configurations (as well as one uncross-linked filament) that were identified as outliers. Unrestricted cross-linking leads to a variety of outliers, including hairpin-like and some that are less severely deformed. Hairpin configurations are more likely with unrestricted cross-linking because two bundles oriented in opposite directions can be cross-linked and coalesce into a single bundle. Thus, a filament that initially spans the two bundles in a horseshoe-like configuration can be forced into an even more unfavorable hairpin configuration when the bundles coalesce. This process is shown in Videos S5, S6, S7, and \$8.

Disentangling the effects of the alignment potential

The alignment potential, U_{xl}^{align} , affects the organization of the actin network by altering the binding kinetics of crosslinkers and by causing bound cross-linkers to impose alignment forces. We investigated the relative importance of these two effects by conducting simulations for which the alignment potential: 1) impacts the binding rate but does not impose a force on the filaments; and 2) does not impact the binding rate but does impose a force on cross-linked filaments. To quantify the effect, we examined the distribution of angles between cross-linked filament links after 400 s (Fig. 10). Restricted cross-linkers give rise to a single

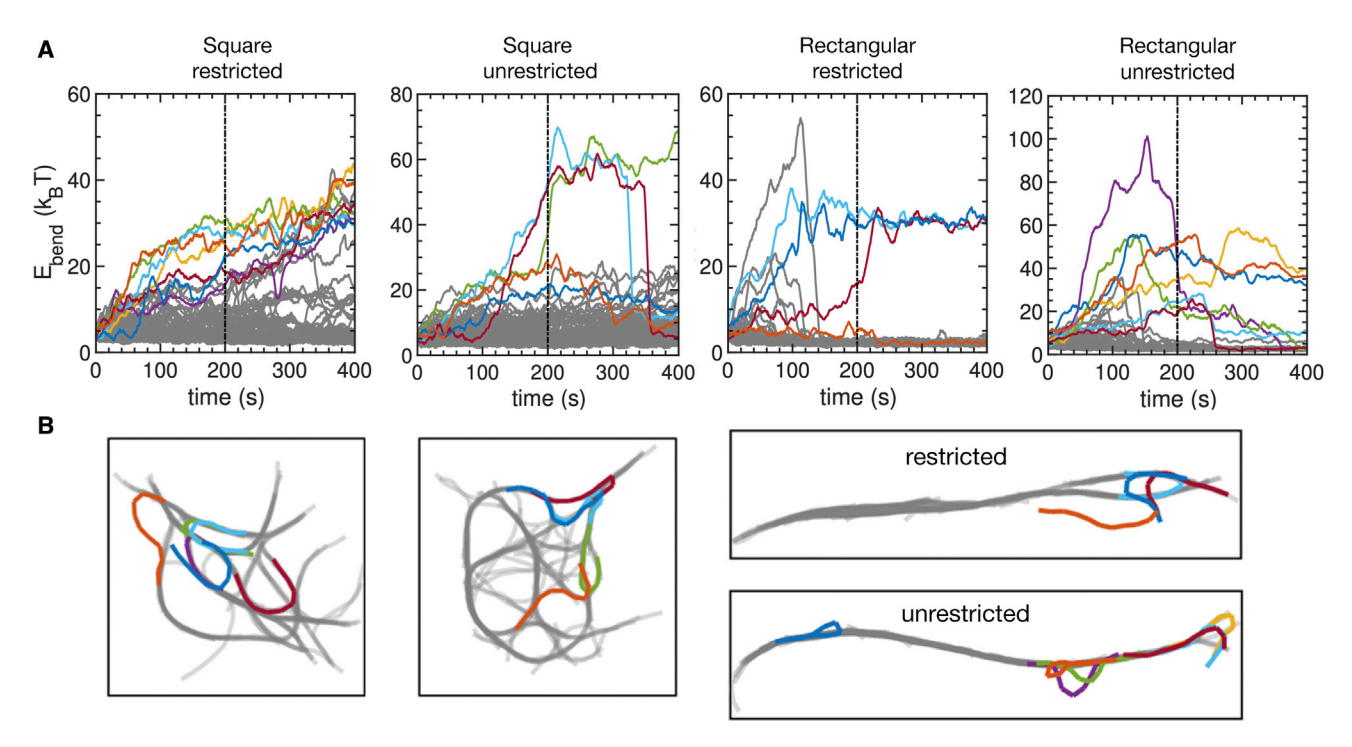


FIGURE 9 (A) Bending energies of individual filaments over the course of a simulation trajectory with 10-µm filaments and 3300 cross-linkers. Filaments with bending energy that fall below the upper fence of the distribution at 200 s (vertical line) are shown in gray. The bending energy of other filaments is shown in other colors. (B) Snapshots of the same trajectories at 200 s. Filaments are shown in the same color as in (A). A corresponding video showing the full trajectory is available for each case (Videos S5, S6, S7, and S8). To see this figure in color, go online.

peak with a maximum at 0, indicating parallel segments. In contrast, unrestricted cross-linkers give rise to a distribution with peaks at 0 and π , indicating parallel and antiparallel segments.

When the alignment potential affects the binding rate but does not impose force, for long filaments, there are no appreciable differences with or without the alignment force (Fig. 10). This indicates that the altered binding kinetics are sufficient to organize the filaments. With shorter filaments, the distribution of angles has more weight at larger angles, indicating that some filaments reorient relative to their cross-linked partner after binding. This is more common with shorter filaments and fewer cross-linkers (Fig. S12) because they have fewer cross-linkers per filament to frustrate their reorientation.

When the alignment potential does not impact the binding rate but imposes a force, there is a sharp decrease in the peak associated with antiparallel filaments compared with unrestricted binding (Fig. 10). However, there is a prominent tail at large angles, which is most pronounced for long filaments because frustration in binding can be hard to relax due to the large number of cross-linkers per filament.

These results demonstrate that modified binding kinetics are sufficient to significantly restrict the angle between filaments over the course of a 400-s trajectory. However, imparting a force on filaments helps to maintain the angle between filaments, especially for smaller numbers of cross-linkers and shorter filaments.

CONCLUSION

Cells utilize various ACPs with different biophysical properties. This raises questions about the impact of different ACPs on the dynamics and organization of the cytoskeleton and their functional roles in cellular processes. Different ACPs also present an opportunity in reconstituted systems, where different cross-linkers could be used to control features of actin networks, with implications in applications such as artificial cells and transport in synthetic systems (43). However, fundamental questions still remain about how properties of cross-linkers and physical confinement impact cytoskeletal dynamics and organization.

Our work here demonstrates how the assembly of filaments into cross-linked networks is influenced by the mode of cross-linker binding and the shape of its physical confinement. To better understand these features, we varied the length of filaments and number of cross-linkers while focusing on two types of cross-linkers: restricted cross-linkers that preferentially cross-link locally aligned filaments and unrestricted cross-linkers that cross-link filaments without regard for relative filament orientation.

Introducing cross-linkers into a system of filaments induced aggregation and bundling of the filaments. The dynamics were characterized by a fast response at early times followed by slower changes at longer times. The fast initial response resulted from aggregation of nearby filaments into bundles, whereas the slower dynamics reflected relaxation

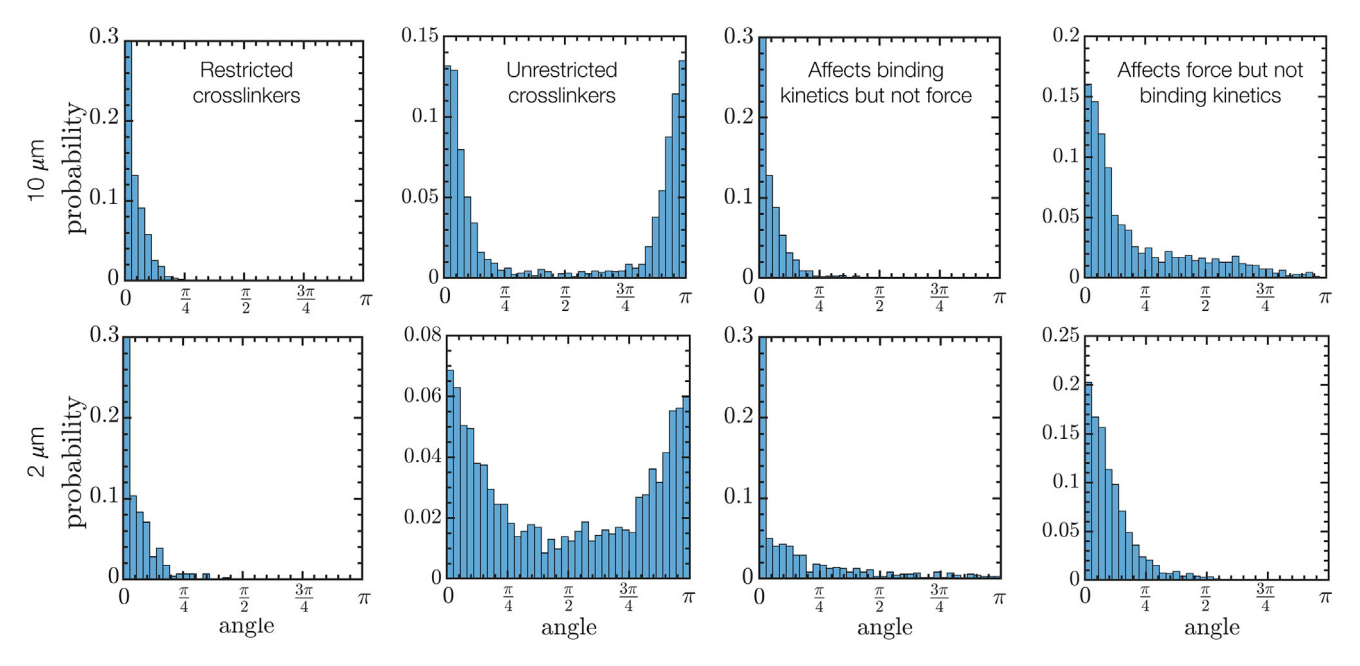


FIGURE 10 Distributions of angles between cross-linked filament links for networks of 10- and 2-\mu m filaments (top and bottom row, respectively) with 825 cross-linkers. Results correspond to networks at 400 s. Each distribution is constructed with data from three simulation trajectories. To see this figure in color, go online.

of cross-linked filaments and bundles and their continued reorganization into larger bundles. With large numbers of cross-linkers and sufficiently long filaments, we observed the formation of highly connected and deformed bundles with loops and filaments spanning between bundles. This behavior was promoted by unrestricted cross-linkers and is reflected in slower aggregation (Fig. 6) and a higher average bending energy of filaments (Fig. 8). Increasing the aspect ratio of the system promoted aggregation of filaments into fewer, better-defined bundles that aligned with the long dimension of the system. It was surprising to observe elevated bending energies with relatively straight bundles in rectangular confinement. This revealed highly deformed "outlier" filaments with anomalously high bending energies. The formation of these filaments was promoted by unrestricted cross-linking and square confinement. Although our study makes approximations, such as neglecting excluded volume (44) and the breaking of buckled filaments (45), we expect dynamics of filaments to be dominated by cross-linking, with slow relaxation of filaments largely governed by the reorganization of cross-linkers. We suggest that it would be interesting to design experiments to look for such highly deformed filaments in highly cross-linked actin networks.

A number of the observations presented here are consistent with experimental results. Large numbers of cross-linkers in square confinement produced highly interconnected, deformed bundles of long filaments and short, isolated bundles of short filaments. These structures are similar to those observed in experiments in which filamin was used to cross-link actin filaments of various lengths in quasi-2D microfluidic chambers (39). Additionally, the alignment of bundles with the long axis of the system in rectangular confinement is consistent with experiments in which bundled actin filaments align with the long axis under confinement (31,32). We also showed that large numbers of unrestricted cross-linkers caused slower aggregation of filaments when the filaments were sufficiently long. This phenomenon is similar to the dynamic arrest observed in Falzone et al., where faster growing filaments cross-linked by α -actinin generated slower bundle formation (46). In the simulations, this slower aggregation is due to unrestricted cross-linkers quickly cross-linking filaments into unfavorable conformations at early times. Combined with the semiflexible nature of filaments, this leads to frustration within the network that is difficult to relax, making further bundling more challenging. This is also consistent with accumulation and slow relaxation of stress observed in bundled networks (47,48). Subsequent relaxation of the deformed filaments is likely controlled by thermally driven cross-linker unbinding events (48).

Our results provide insight into mechanisms contributing to the organization of actin filaments in cells and in synthetic systems. In cells, the cytoskeleton is influenced by additional factors, including forces imparted by molecular motors involved in the transport of organelles (49–52). Interesting future directions for computational studies include investigating the impact of multiple types of ACPs concurrently and studying the interplay between organelle transport and the organization of cross-linked actin networks.

SUPPORTING MATERIAL

Supporting Material can be found online at https://doi.org/10.1016/j.bpj. 2022.11.2944.

AUTHOR CONTRIBUTIONS

O.H.A. and S.M.A. designed research. O.H.A. performed research. O.H.A. and S.M.A. analyzed data and wrote the manuscript.

ACKNOWLEDGMENTS

This work was supported by National Science Foundation grant MCB-1715794.

DECLARATION OF INTERESTS

The authors declare no competing interests.

REFERENCES

- 1. Peremyslov, V. V., A. I. Prokhnevsky, and V. V. Dolja. 2010. Class XI myosins are required for development, cell expansion, and F-actin organization in Arabidopsis. Plant Cell. 22:1883-1897. https://doi.org/ 10.1105/tpc.110.076315.
- 2. Park, E., and A. Nebenführ. 2013. Myosin XIK of Arabidopsis thaliana Accumulates at the root hair tip and is required for fast root hair growth. PLoS One. 8:e76745.
- 3. Madison, S. L., M. L. Buchanan, ..., A. Nebenführ. 2015. Class XI myosins move specific organelles in pollen tubes and are required for normal fertility and pollen tube growth in Arabidopsis. Plant Physiol. 169, 01161. https://doi.org/10.1104/pp.15.01161.
- 4. Qu, X., Y. Jiang, ..., S. Huang. 2014. Organization and regulation of the actin cytoskeleton in the pollen tube. Front. Plant Sci. 5:786. http:// journal.frontiersin.org/article/10.3389/fpls.2014.00786/abstract.
- 5. Thomas, C., S. Tholl, ..., A. Steinmetz. 2009. Actin bundling in plants. Cell Motil. Cytoskeleton. 66:940–957. https://doi.org/10.1002/cm.
- 6. Pollard, T. D., L. Blanchoin, and R. D. Mullins. 2000. Molecular mechanisms controlling actin filament dynamics in nonmuscle cells. Annu. Rev. Biophys. Biomol. Struct. 29:545-576. https://doi.org/10.1146/annurev.biophys.29.1.545.
- 7. Staiger, C. J., M. B. Sheahan, ..., L. Blanchoin. 2009. Actin filament dynamics are dominated by rapid growth and severing activity in the Arabidopsis cortical array. J. Cell Biol. 184:269-280.
- 8. Lieleg, O., M. M. A. E. Claessens, ..., A. R. Bausch. 2007. Mechanics of bundled semiflexible polymer networks. Phys. Rev. Lett. 99, 088102. https://doi.org/10.1103/PhysRevLett.99.088102.
- 9. Lieleg, O., K. M. Schmoller, ..., A. R. Bausch. 2009. Structural polymorphism in heterogeneous cytoskeletal networks. Soft Matter. 5:1796-1803.
- 10. Purdy, K. R., J. R. Bartles, and G. C. L. Wong. 2007. Structural polymorphism of the actin-espin system: a prototypical system of filaments and linkers in Stereocilia. Phys. Rev. Lett. 98, 058105. https://doi.org/ 10.1103/PhysRevLett.98.058105.
- 11. Schmoller, K. M., O. Lieleg, and A. R. Bausch. 2009. Structural and viscoelastic properties of actin/filamin networks: cross-linked versus bundled networks. Biophys. J. 97:83-89. https://www.sciencedirect. com/science/article/pii/S0006349509008984.
- 12. Courson, D. S., and R. S. Rock. 2010. Actin cross-link assembly and disassembly mechanics for α -actinin and fascin. J. Biol. Chem. 285:26350-26357.

- 13. Lieleg, O., M. M. A. E. Claessens, and A. R. Bausch. 2010. Structure and dynamics of cross-linked actin networks. Soft Matter. 6:218-225. http://xlink.rsc.org/?DOI=B912163N.
- 14. Tominaga, M., E. Yokota, ..., T. Shimmen. 2000. The role of plant villin in the organization of the actin cytoskeleton, cytoplasmic streaming and the architecture of the transvacuolar strand in root hair cells of Hydrocharis. Planta. 210:836-843. https://doi.org/10.1007/ s004250050687.
- 15. Cavanna, F., and J. Alvarado. 2021. Quantification of the mesh structure of bundled actin filaments. Soft Matter. 17:5034-5043. https:// doi.org/10.1039/D1SM00428J.
- 16. Nguyen, L. T., W. Yang, ..., L. S. Hirst. 2009. Molecular dynamics simulation of F-actin reveals the role of cross-linkers in semi-flexible filament assembly. Soft Matter. 5:2033. http://xlink.rsc.org/?DOI=
- 17. Nguyen, L. T., and L. S. Hirst. 2011. Polymorphism of highly crosslinked F-actin networks: probing multiple length scales. Phys. Rev. E. 83:031910-031919.
- 18. Borukhov, I., R. F. Bruinsma, ..., A. J. Liu. 2005. Structural polymorphism of the cytoskeleton: a model of linker-Assisted filament aggregation. Proc. Natl. Acad. Sci. USA. 102:3673-3678. http://arxiv.org/ abs/cond-mat/0504708.
- 19. Foffano, G., N. Levernier, and M. Lenz. 2016. The dynamics of filament assembly define cytoskeletal network morphology. Nat. Commun. 7, 13827. http://www.nature.com/articles/ncomms13827
- 20. Freedman, S. L., S. Banerjee, ..., A. R. Dinner. 2017. A versatile framework for simulating the dynamic mechanical structure of cytoskeletal networks. Biophys. J. 113:448-460. https://doi.org/10.1016/j.bpj. 2017.06.003.
- 21. Müller, K. W., C. J. Cyron, and W. A. Wall. 2015. Computational analysis of morphologies and phase transitions of cross-linked, semi-flexible polymer networks. Proc. R. Soc. A. 471, 20150332. https://doi. org/10.1098/rspa.2015.0332.
- 22. Cyron, C. J., K. W. Müller, ..., R. F. Bruinsma. 2013. Equilibrium phase diagram of semi-flexible polymer networks with linkers. Euro Phys. Lett. 102, 38003. https://doi.org/10.1209/0295-5075/102/38003.
- 23. Ma, R., and J. Berro. 2018. Structural organization and energy storage in crosslinked actin assemblies. PLoS Comput. Biol. 14:e1006150.
- 24. Nedelec, F., and D. Foethke. 2007. Collective Langevin dynamics of flexible cytoskeletal fibers. New J. Phys. 9:427.
- 25. Maxian, O., A. Donev, and A. Mogilner. 2022. Interplay between Brownian motion and cross-linking controls bundling dynamics in actin networks. Biophys. J. 121:1230-1245. https://www.science direct.com/science/article/pii/S0006349522001540.
- 26. Popov, K., J. Komianos, and G. A. Papoian. 2016. MEDYAN: mechanochemical simulations of contraction and polarity alignment in actomyosin networks. PLoS Comput. Biol. 12:e1004877. https://doi.org/10. 1371/journal.pcbi.1004877.
- 27. Freedman, S. L., G. M. Hocky, ..., A. R. Dinner. 2018. Nonequilibrium phase diagrams for actomyosin networks. Soft Matter. 14:7740-7747. http://xlink.rsc.org/?DOI=C8SM00741A.
- 28. Freedman, S. L., C. Suarez, ..., G. M. Hocky. 2019. Mechanical and kinetic factors drive sorting of F-actin cross-linkers on bundles. Proc. Natl. Acad. Sci. USA. 116:16192–16197. http://www.ncbi.nlm. nih.gov/pubmed/31346091. http://www.pubmedcentral.nih.gov/article render.fcgi?artid=PMC6697872.
- 29. Bashirzadeh, Y., S. A. Redford, ..., A. P. Liu. 2021. Actin cross-linker competition and sorting drive emergent GUV size-dependent actin network architecture. Commun. Biol. 4:1136. https://doi.org/10.1038/ s42003-021-02653-6.
- 30. Cosentino Lagomarsino, M., C. Tanase, ..., M. Dogterom. 2007. Microtubule organization in three-dimensional confined geometries: evaluating the role of elasticity through a combined in vitro and modeling approach. Biophys. J. 92:1046-1057. https://doi.org/10. 1529/biophysj.105.076893.

- 31. Soares E Silva, M., J. Alvarado, ..., G. H. Koenderink. 2011. Self-organized patterns of actin filaments in cell-sized confinement. Soft Matter. 7:10631-10641. http://xlink.rsc.org/?DOI=c1sm06060k.
- 32. Alvarado, J., B. M. Mulder, and G. H. Koenderink. 2014. Alignment of nematic and bundled semiflexible polymers in cell-sized confinement. Soft Matter. 10:2354-2364.
- 33. Limozin, L., M. Bärmann, and E. Sackmann. 2003. On the organization of self-assembled actin networks in giant vesicles. Eur. Phys. J. E Soft Matter. 10:319-330. http://link.springer.com/10.1140/epje/i2002-10118-9.
- 34. Tsai, F.-C., S. Roth, ..., G. Koenderink. 2014. Biomimetic liposome model systems to study cell shape control by the cytoskeleton. Adv. Planar Lipid Bilayers Liposomes. 19:139–173.
- 35. Hase, M., and K. Yoshikawa. 2006. Structural transition of actin filament in a cell-sized water droplet with a phospholipid membrane. J. Chem. Phys. 124:104903.
- 36. Claessens, M. M. A. E., R. Tharmann, ..., A. R. Bausch. 2006. Microstructure and viscoelasticity of confined semiflexible polymer networks. Nat. Phys. 2:186-189. https://doi.org/10.1038/nphys241.
- 37. Mirzaeifard, S., and S. M. Abel. 2016. Confined semiflexible polymers suppress fluctuations of soft membrane tubes. Soft Matter. 12:1783-1790. https://www.ncbi.nlm.nih.gov/pubmed/26700763.
- 38. Vetter, R., F. K. Wittel, and H. J. Herrmann. 2014. Morphogenesis of filaments growing in flexible confinements. Nat. Commun. 5:4437. https://doi.org/10.1038/ncomms5437.
- 39. Deshpande, S., and T. Pfohl. 2015. Real-time dynamics of emerging actin networks in cell-mimicking compartments. PLoS One. 10:
- 40. Adeli Koudehi, M., D. M. Rutkowski, and D. Vavylonis. 2019. Organization of associating or cross-linked actin filaments in confinement. Cytoskeleton. 76:532-548.
- 41. Allen, M. P., and D. J. Tildesley. 1989. Computer Simulation of Liquids. Clarendon Press.

- 42. Newman, M. E. J. 2004. Fast algorithm for detecting community structure in networks. Phys. Rev. E Stat. Nonlin. Soft Matter Phys. 69, 066133. https://doi.org/10.1103/PhysRevE.69.066133.
- 43. Bashirzadeh, Y., and A. P. Liu. 2019. Encapsulation of the cytoskeleton: towards mimicking the mechanics of a cell. Soft Matter. 15:8425-8436. https://doi.org/10.1039/C9SM01669D.
- 44. Müller, K. W., R. F. Bruinsma, ..., A. J. Levine. 2014. Rheology of semiflexible bundle networks with transient linkers. Phys. Rev. Lett. 112, 238102. https://doi.org/10.1103/PhysRevLett.112.238102.
- 45. Murrell, M. P., and M. L. Gardel. 2012. F-actin buckling coordinates contractility and severing in a biomimetic actomyosin cortex. Proc. Natl. Acad. Sci. USA. 109:20820-20825.
- 46. Falzone, T. T., M. Lenz, ..., M. L. Gardel. 2012. Assembly kinetics determine the architecture of α-actinin cross-linked F-actin networks. Nat. Commun. 3:861–869. https://doi.org/10.1038/ncomms1862.
- 47. Schmoller, K. M., O. Lieleg, and A. R. Bausch. 2008. Internal stress in kinetically trapped actin bundle networks. Soft Matter. 4:2365–2367.
- 48. Lieleg, O., J. Kayser, ..., A. R. Bausch. 2011. Slow dynamics and internal stress relaxation in bundled cytoskeletal networks. Nat. Mater. 10:236-242.
- 49. Houdusse, A., and H. L. Sweeney. 2016. How myosin generates force on actin filaments. Trends Biochem. Sci. 41:989-997. https:// linkinghub.elsevier.com/retrieve/pii/S0968000416301529
- 50. Mlynarczyk, P. J., and S. M. Abel. 2019. First passage of molecular motors on networks of cytoskeletal filaments. Phys. Rev. E. 99, 022406. https://doi.org/10.1103/PhysRevE.99.022406.
- 51. Jung, W., L. A. Fillenwarth, ..., T. Kim. 2020. Collective and contractile filament motions in the myosin motility assay. Soft Matter. 16:1548-1559. http://xlink.rsc.org/?DOI=C9SM02082A.
- 52. Agrawal, A., Z. C. Scott, and E. F. Koslover. 2022. Morphology and transport in eukaryotic cells. Annu. Rev. Biophys. 51:247-266. https://doi.org/10.1146/annurev-biophys-111121-103956.